# Optimizing Substrate-Mediated Plasmon Coupling toward High-Performance Plasmonic Nanowire Waveguides

**Shunping Zhang[†] and Hongxing Xu[†,‡,*]**

[†]Beijing National Laboratory for Condensed Matter Physics and Institute of Physics, Chinese Academy of Sciences, Box 603-146, Beijing 100190, China and
[‡]Division of Solid State Physics/The Nanometer Structure Consortium, Lund University, Box 118, S-22100, Lund, Sweden

**ABSTRACT**

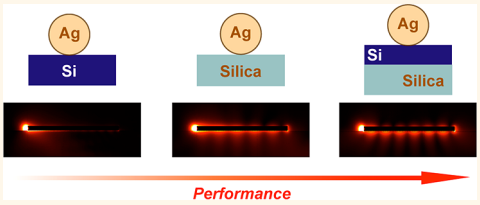


**Seeking better plasmonic waveguides is of critical importance for minimizing photonic circuits into the nanometer scale. We have made a theoretical study of the properties of surface plasmon polaritons in a metallic nanowire over substrate (NWOS) configuration. The dielectric substrate breaks the symmetry of the system and mediates the coupling of different primary wire plasmons. The lowest order hybridized mode can be used for subwavelength plasmonic waveguiding for NWOS with thin wire, for a low-permittivity substrate, and in the shorter wavelength region. For NWOS with a high-permittivity substrate, leaky radiation into the substrate raises the propagation losses so that the propagation distance is shorter in the longer wavelength region. By simply adding a high-permittivity layer onto the low-permittivity substrate, we show that leaky radiation can be blocked and high-performance plasmonic waveguiding can be extended to the near-infrared region. Importantly, the NWOS configuration is compatible with current silicon technologies and can be designed into various deep subwavelength active devices such as electro-optical or all-optical modulators.**

**KEYWORDS:** SPPs · nanowire · plasmonic waveguides · substrate · silicon compatible

The downscaling of photonic devices remains one of the major challenges in nanophotonics. Metallic waveguides are promising candidates to achieve subdiffraction waveguiding since they support surface plasmon polaritons (SPPs), propagating electromagnetic excitations associated with the collective motions of conduction electrons confined to metal–dielectric interfaces.[1] So far, various types of metallic structures have been demonstrated to support propagating SPPs with potential for constructing subdiffraction photonic circuits, including metallic wires,[2−5] nanoparticle chains,[6] wedges,[7] V-shaped grooves or slots on films,[8,9] and hybridized waveguides.[10] The main obstacle for using such plasmonic structures is the severe losses associated with the metal components, resulting in a short propagation length, typically on the order of several micrometers in the visible range. Therefore, searching for high-performance plasmonic waveguides with a longer propagation length and smaller modal area represents a topic of intense interest.[1] By exploiting the interactions between adjacent components, pioneers have succeeded in achieving high figure of merit (FoM) waveguiding in dielectric wires on a metal substrate and in coupling metallic structures.[5,10,11] The idea works because the strong coupling between the closely spaced components dramatically squeezes the plasmon modal volume into a deep subwavelength space, while preserving a modest propagation length. In terms of fabrication, these gap modes require ultrasmooth metal surfaces or nanowires aligned with nanometer precision.[5,12] On the other hand, well-developed aqueous solution procedures or template-based methods are now available for high-throughput fabrication of crystallized silver/gold nanowires with a controlled shape and atomic-scale smooth surfaces.[13,14] Integration of such high-quality nanowires can reduce additional losses due to the polycrystalline nature of the deposited metal by using top-down fabrication techniques. In this article, we present a theoretical study of the SPPs supported in a metallic nanowire over substrate (NWOS) configuration. We show that by using a

* Address correspondence to hxxu@iphy.ac.cn.

Received for review June 21, 2012 and accepted August 14, 2012.

**Published online August 14, 2012**
**10.1021/nn302755a**

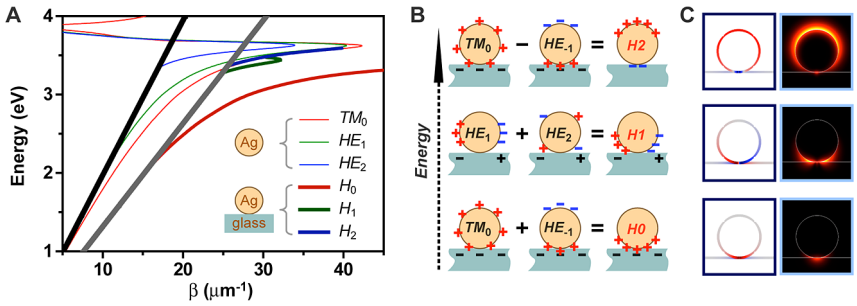


**Figure 1. Substrate-mediated surface plasmon hybridization. (A) Dispersion relationship of the three lowest order modes on a silver nanowire ($R$ = 100 nm) in air (thin lines) and supported on an air−glass interface (thick lines). The black and gray lines are the light lines in air and glass, respectively. (B) Schematic drawing of how different primary wire plasmons interact through the dielectric substrate. (C) Normalized surface charge contour (left) and time-averaged power flow (right) of the three hybridized modes with equal phase constant $\beta = 28\,\mu m^{-1}$. Top to bottom: $H_2$ (3.432 eV), $H_1$ (3.359 eV), and $H_0$ (2.988 eV). The nanowire ($R$ = 100 nm) is supported on a glass substrate.**

layered dielectric substrate, leaky radiation can be blocked so that NWOS can be used for plasmonic waveguiding in both the visible and near-infrared regions. More importantly, this structure is fully compatible with semiconductor fabrication techniques, but with a low fabrication barrier. This finding provides a simple prototype for on-chip optical interconnects and other integrated active devices.

Metallic nanowires have been a subject of intense interest for subwavelength optical guiding or circuitry in the past two decades.[2−4,15−21] Though the properties of SPPs on a cylindrical wire in homogeneous medium have been known analytically for a long time, these solutions are not valid when the wire is brought into the vicinity of a dielectric substrate due to the breaking of the cylindrical symmetry. Despite the fact that most of the experimental investigations[3,4,15,21−27] involve nanowires deposited on a dielectric substrate, little is known about how the wire plasmons interact with a nearby dielectric substrate.[28,29] It has been shown that the dielectric environment created by an asymmetric interface can strongly modify the surface plasmon resonances of a nearby metallic nanoparticle, such as shifting their energies, creating new modes, and changing the resonant line shapes and/or radiation patterns.[30−35] The degree of interactions with the substrate depends on the permittivity of the substrate, the gap distance, and the geometry of the contact between the metal and the substrate.[33,36] As will be shown below for one-dimensional metallic nanowire, an optimized degree of interaction with the substrate is critical to achieve high-performance plasmonic waveguiding. This requires a well-designed substrate and gap distance, in combination with a nanowire with a proper size and cross section.

## RESULTS AND DISCUSSION

To model the metallic waveguides, we use a mode solver integrated with a commercial finite element method package (COMSOL Multiphysics, 3.5a). Convergence tests were carried out by refining the mesh and enlarging the computation domain until all the calculated parameters remain unchanged. In order to simulate infinite air and substrate regions, the computation domain was truncated by a perfectly matched layer (PML) to reduce reflections. To describe the silver metal, we use experimentally measured permittivity data (JC),[37] while a parameter fit to, and interpolation of, the JC data was adopted for describing the wavelength dependence of the dielectric function.[38] The glass substrate was modeled using a refractive index of $n_s = 1.5$. The properties of a SPP mode are characterized by a complex wave vector, $\tilde{\mathbf{k}}$, whose parallel component $k_{\|} = \beta + i\alpha$ defines the propagating constant with $\beta$ and $\alpha$ the phase and attenuation constants, respectively. The propagation length $L$ is obtained from $L = 1/2\alpha$, while the mode area $A$ is defined as a minimum area that contains as much as $1 - 1/e^2$ of the total modal energy[39] (see Methods). A good plasmonic waveguide is a combination of long propagation length and high mode confinement. Therefore, the ratio between the propagation length $L$ and the effective mode diameter $2(A/\pi)^{1/2}$ defines a unitless FoM as $\mathrm{FoM} = (1/2)L(\pi/A)^{1/2}$.[40]

To ease the mode assignments, we choose nanowires with a cylindrical cross section. Figure 1A shows the dispersion relationship of the three lowest order modes on a silver nanowire (radius $R$ = 100 nm), both in air and at the air−glass interface. Due to the cylindrical symmetry, the nanowire in air supports SPP modes that are well characterized by the azimuthal quantum number $m$ ($m$ = 0, ± 1, ± 2, ...). According to their major field components (electric or magnetic), these modes are assigned as $TM_0$, $HE_{\pm1}$, $HE_{\pm2}$, and so on.[41] However, the cylindrical symmetry is broken when a dielectric substrate is present. The substrate mediates the coupling between primary SPP modes *via* polarized charges on the substrate surface, leading to a new set of hybridized modes (denoted $H_0$, $H_1$, $H_2$, ...). As shown in Figure 1A, the fundamental mode ($H_0$) in the NWOS system is located at the bottom right compared to the primary $TM_0$ mode. It is also revealed in Figure S2

by using the free electron model for silver ($\varepsilon_{Ag} = 1 - \omega_B^2/\omega^2$, $\omega_B$ is the bulk plasmon frequency of silver) that the corresponding surface plasmon frequency is shifted from $\omega_B/\sqrt{2}$ ($TM_0$) to $\omega_B/(1 + n_s^2)^{1/2}$ ($H_0$) when the nanowire is moved from air to being in contact with the substrate ($n_s$ is the refractive index of the substrate). Another important feature of the NWOS system is that below a critical energy the phase constant $\beta$ of the SPP modes becomes smaller than that for light in the substrate, even for the otherwise no-cutoff fundamental mode ($TM_0$). The modes then become leaky (radiative) into the substrate and the propagation losses rise.[28,42] These leaky modes enable the experimental observations of the SPPs *via* leaky mode microscopy.[25] Furthermore, for a nanowire in air, the $HE_{\pm1}$ modes are degenerate, corresponding to a collective surface charge oscillating perpendicular to the wire axis in a horizontal or vertical plane.[43] However, the interaction with the substrate lifts the degeneracy of the two modes, leading to two new hybridized modes ($H_1$ and $H_2$).

The substrate effect can be qualitatively interpreted using an "image charge" picture in the quasi-static limit.[35] For structures with one infinitely extended dimension, the substrate-mediated coupling takes place between primary modes with equal $\beta$. Figure 1B shows schematically how the primary wire plasmons interact *via* the dielectric substrate underneath, with those coupling to higher order modes ($m > 2$) not shown in the figure. Obviously, the otherwise degenerate $HE_{\pm1}$ modes interact predominantly with different primary wire modes and evolve gradually into the $H_1$ and $H_2$ modes as the substrate-mediated coupling is getting stronger. The $H_1$ mode comes from an in-phase (inducing the same polarized charges on the substrate surface) coupling of the $HE_1$ and $HE_2$ modes, while the $H_2$ mode comes mainly from an out-of-phase (canceling their induced polarized charges on the substrate surface) coupling between the $TM_0$ and $HE_{-1}$ mode. According to the plasmon hybridization,[44] the coupling with the $HE_2$ ($TM_0$) mode will result in a red-shift (blue-shift) for the $H_1$ ($H_2$) mode compared to the original $HE_{\pm1}$ mode. That is why the $H_2$ mode has a higher energy than the $H_1$ mode, as shown in Figure 1A and B. Besides the asymmetric coupling to the substrate, the pure dielectric screening effect and the interactions with other higher order modes can further reduce the energies, which explains why both the energies of the $H_1$ and $H_2$ modes are smaller than that of the original $HE_{\pm1}$ mode. Figure 1C shows the calculated surface charges and the time-averaged power flow distributions of the three lowest order hybridized modes. The charge plots agree with those in Figure 1B, further confirming our understanding of the interactions of different wire plasmons *via* the substrate. Compared with the primary $HE_1$ ($HE_{-1}$) mode, most of the energy of the hybridized $H_1$ ($H_2$) mode is located toward the bottom (top) of the nanowire. When excited by a focus laser at the nanowire terminal, the $H_0$ and $H_2$ mode can be launched if the incident electric field is polarized parallel to the nanowire axis, while the $H_1$ can be excited for perpendicular incident polarization.[43] It is the $H_0$ and $H_2$ modes, excited under parallel polarization, that are responsible for the previous experimental observations of the plasmon beatings in the NWOS configuration.[23] Originating from the $HE_{\pm1}$ mode, the $H_1$ and $H_2$ modes preserve, to a certain degree, the unidirectional emission characteristic at the terminals,[45] which explains the experimental observations by Shegai *et al.*[24,46]

The mode area of the $TM_0$ mode can be shrunk as the nanowire gets smaller, at the price of larger propagation losses. The behavior of the $HE_{\pm1}$ modes, however, is the opposite.[45] Such a trade-off between mode confinement and propagation distance is well known for plasmonic waveguides. Figure 2A shows the propagation length $L$, mode area $A$, and FoM of the $H_0$ mode for a nanowire ($R$ = 40 nm) near a dielectric substrate with a refractive index of $n_s$. Interestingly, the propagation length of the $H_0$ mode in NWOS is comparable to or even larger than that of the $TM_0$ mode in air. This is actually the consequence of the hybridization to the low-loss $HE_{-1}$ mode. However, the reduced propagation loss is accompanied by an increase in the mode area so that the trade-off between mode confinement and propagation distance remains. The FoM is smaller for the $H_0$ mode in NWOS compared to the $TM_0$ mode in air. Another definition of the mode area will result in the opposite behavior (see Figure S3).

Figure 2A also reveals that as the wavelength increases, the propagation length and mode area increase. This is due to the fact that the real part of the dielectric constant of silver metal becomes more negative, so that the penetration depth into the metal is getting smaller, resulting in a smaller ohmic loss. However, the presence of the substrate prevents the system from working in the long-wavelength regime: above a critical wavelength, the $H_0$ mode becomes leaky. Note that once the mode is leaky, the definition of mode area becomes problematic and the propagation length obtained in our simulation models becomes inaccurate. That is why the plots are cut in the long-wavelength region in Figure 2A. The spectral region clamped between the surface plasmon frequency and this bound-to-leaky transition point defines a window where the $H_0$ mode is nonradiative: a spectral working window. Figure 2A also shows that for NWOS with a larger gap ($G$ = 5 nm), a thicker nanowire ($R$ = 60 nm), or a higher refractive index substrate ($n_s$ = 2.5), this window becomes narrowed. Even within the spectral working window, the coupling with a high-permittivity substrate is so strong that the mode becomes highly localized and the propagation losses

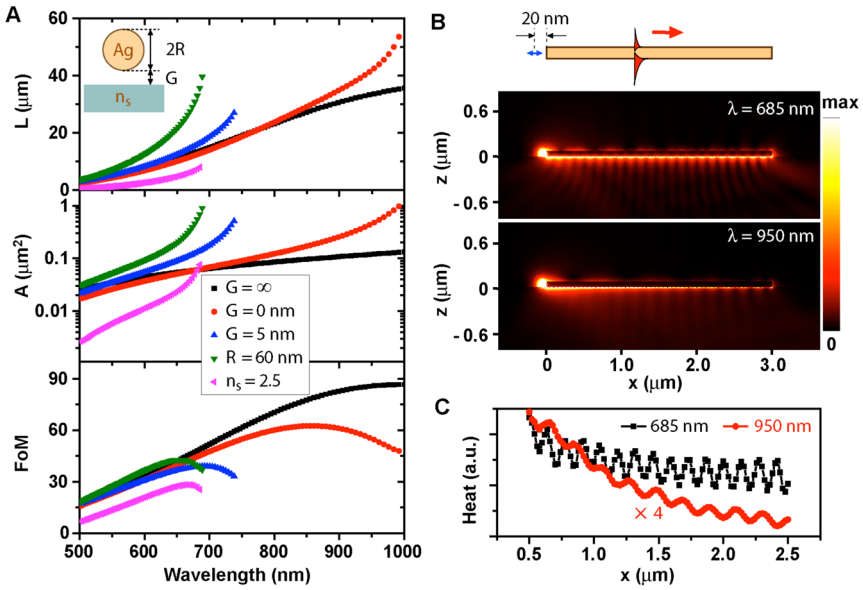


**Figure 2. (A) Propagation length *L* (top), mode area *A* (middle), and FoM (bottom) of the fundamental mode as a function of wavelength. Inset: Cross section of the NWOS configuration. The nanowire ($R$ = 40 nm) is separated from the glass substrate ($n_s$ = 1.5) by a gap $G = \infty$ (black square), 0 nm (red circle), and 5 nm (blue up triangle). The cases for a thicker nanowire ($R$ = 60 nm, $G$ = 0 nm, $n_s$ = 1.5, green down triangle) or higher refractive index substrate ($R$ = 40 nm, $G$ = 0 nm, $n_s$ = 2.5, magenta left triangle) are also compared. Electric field (B) and Joule heating (C) distribution for NWOS configuration in the bound ($\lambda$ = 685 nm) and leaky ($\lambda$ = 950 nm) regions, $R$ = 40 nm, $n_s$ = 2.5. The position and orientation of the exciting dipole are indicated by a blue arrow in B.**

increase significantly. The occurrence of such high loss features in the entire spectral range represents the major obstacle for the metal waveguides to be directly incorporated with a high-permittivity substrate.[29]

To get an intuitive view of the influence of the leaky loss, Figure 2B and C compare the NWOS in the bound and leaky region. Modeled by an oscillating current segment, a point dipole source sitting 20 nm away from the terminal of a 3 $\mu$m long Ag nanowire is used to launch the $H_0$ SPP. There are three channels that the $H_0$ mode eventually dissipates into: Joule heating within the metal region, radiation leaking into the substrate, and the cavity loss due to the end facets. Figure 2B clearly shows the absence and the presence of leakage radiation for $\lambda$ = 685 and 950 nm, respectively. Since the Joule heating is proportional to how much electromagnetic energy resides in the nanowire, we plot the heat in Figure 2C to better compare the propagation losses. Obviously, the leakage radiation raises the propagation losses so that the Fabry-Pèrot interference is less apparent and the heat decays faster along the nanowire. It is noted that when leaky loss dominates over the dissipative loss, the wavelength dependence of the propagation losses will be reversed; that is, the longer the wavelength, the larger the propagation losses will be. This is a marked difference from SPPs in a bound region, where the opposite is true.[18,22,27]

To overcome the leaky problem, we propose an alternative structure by simply adding a high refractive index dielectric layer onto a low refractive index substrate, as shown in the inset of Figure 3A. We chose silicon ($n_{spacer}$ = 3.48) on top of silica ($n_s$ = 1.46) substrates, aiming for Si-compatible devices. The high refractive index layer induces stronger substrate-mediated coupling of the wire plasmons, which shifts the dispersion curve of the $H_0$ mode to the bottom right of the light line in the low refractive index substrate. The combined effect of the layered substrate is to provide an optical barrier blocking the leaky radiation. Figure 3A shows the propagation length *L*, mode area *A*, and FoM of the $H_0$ mode as a function of the radius of a nanowire for different spacer thicknesses *T* at the telecom wavelength ($\lambda$ = 1550 nm). For NWOS without the silicon layer, the $H_0$ mode becomes leaky for thicker nanowires. The thin silicon layer is to make the $H_0$ mode bound in the whole range. The benefit of the optically dense layer is illustrated in Figure 3B and C, which compare the NWOS with (i) a 30 nm Si layer on a silica substrate, (ii) a silica substrate, and (iii) a Si substrate. Clear Fabry-Pèrot interference in Figure 3B(i) is a strong indication of long propagation distance compared to the nanowire length. The degraded performance of (ii) is clearly due to the leaky radiation, which becomes even worse for nanowires on a high refractive index substrate (iii).

The beauty of the NWOS configuration is that when active materials are incorporated into the substrate, deep subwavelength functionalized devices such as electro-optical or all-optical modulators can be designed. The NWOS configuration serves as a prototype for CMOS-compatible plasmon interconnects. The reliability of the NWOS configuration as active devices

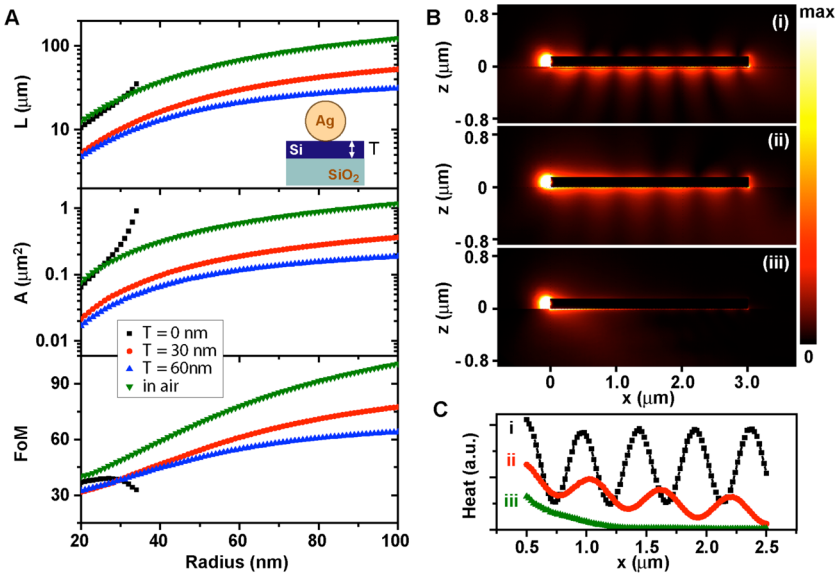


**Figure 3. Layered substrate for plasmonic waveguide in the telecom wavelength ($\lambda$ = 1550 nm). (A) Propagation length *L* (top), mode area *A* (middle), and FoM (bottom) of the $H_0$ mode as a function of the nanowire radius. The nanowire is sitting on top of a silica substrate ($n_s$ = 1.46) with a Si layer ($n_{spacer}$ = 3.48) of thickness *T* = 0, 30, and 60 nm. The *L*, *A*, and FoM for the $TM_0$ mode for a nanowire in air are also compared (green down triangle). Electric field (B) and Joule heating (C) distribution for NWOS configuration with (i) a Si layer (*T* = 30 nm) on a silica substrate, (ii) a silica substrate, and (iii) a Si substrate. The position and orientation of the exciting dipole are the same as in Figure 2. Permittivity of silver, $\varepsilon_M = -129 + 3.3i$.**

also relies on the fact that the fraction of mode energy distribution inside the active medium could not be too small. For a Si layer of 60 nm thickness in Figure 3A, the energy fraction within the Si layer is larger than 40%. Also, the NWOS is to a large extent experimentally accessible, thanks to various well-developed schemes preparing high-quality metallic nanowires and atomic-flat dielectric substrates. Crystallized metallic nanowires have been demonstrated to have no loss caused by crystal grains and surface roughness.[15] Therefore, the ability to integrate such wires represents an important step toward realistic low-loss plasmonic waveguides.

For a nanowire with a noncircular cross section, the primary modes on the wire will reassemble according to its symmetry group.[25] Unlike a cylindrical wire, a polyhedron wire contains sharp corners that are capable of supporting wedge (corner) modes with significant deep subwavelength characteristics.[7,25,47−49] When the size of the wire is reduced, the wedge modes in neighboring corners start to couple to each other and reassemble into wire-like modes. If the corners are not infinitely sharp, for a significantly thin wire, the coupling between corners becomes dominant so that the modes are fully wire-like. Therefore, the above-mentioned substrate-induced plasmon hybridization applies to nanowires with arbitrary cross sections. The shape of the nanowire can greatly influence the strength of the coupling. Figure 4 compares the effective mode index and the propagation length of the $H_0$ mode in NWOS with circular, square, rectangle, and pentagon wire cross sections. To avoid abrupt structural discontinuities and be comparable with

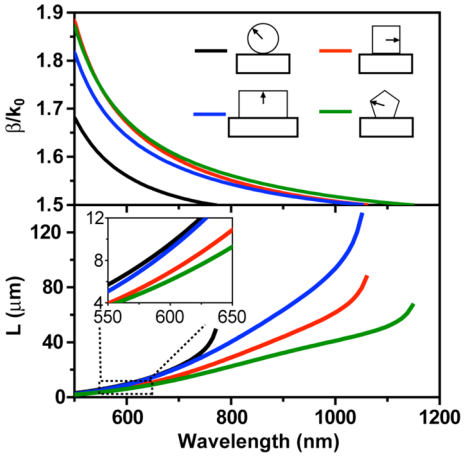


**Figure 4. Phase constant $\beta$ and propagation length *L* as a function of wavelength for nanowires with different cross sections: circular (black), square (red), rectangular (blue), and pentagonal (green). The characteristic size of the wires (indicated as black arrows in the inset) is 50 nm. The width of the rectangle is twice as large as its height, *i.e.*, 200 nm.**

experimental realizations, all the sharp corners in the noncylindrical wire were smoothed to a 2 nm curvature. Unlike a cylindrical wire with a line contact with the substrate below, a noncylindrical wire has a facet contacting with the substrate, which results in a stronger coupling. The hybridized mode is therefore more red-shifted compared to the primary mode in air for a noncylindrical wire, as shown in the top panel of Figure 4. Meanwhile, the bound-to-leaky transition point is shifted to the low-energy region, where the metal has a smaller intrinsic loss. Therefore, a noncylindrical nanowire on a substrate has a larger spectral

working window. However, at a given wavelength where the pure bound mode exists, *e.g.*, $\lambda = 700$ nm, the propagation distance of a cylindrical wire is larger than those of other geometries, *i.e.*, $L = 22.6\ \mu$m (circle), 16.0 $\mu$m (square), 21.6 $\mu$m (rectangle), and 13.2 $\mu$m (pentagon). The rectangular wire has a similar propagation length at the cost of more than a 2-fold increase in the physical dimension. The larger spectral working window for a pentagonal wire than for a square wire comes from the fact that the pentagonal wire has a smaller transverse area used in the calculations (we used equal characteristic lengths).

Besides metallic nanowires with different cross sections, the idea of substrate-mediated plasmon coupling can also apply to thin metal films, where the asymmetric dielectric environment will balance the long-range and short-range SPPs. Though the present analysis of plasmonic waveguiding has been concerned exclusively with the fundamental mode, we note that for thick wires or a rectangular wire with extended width, *i.e.*, a stripe, higher order modes will be shifted to the visible frequency. Even though some of these higher order modes may propagate over a longer distance, the deep subwavelength mode confinements are usually difficult to achieve simultaneously. This means that for realistic applications a suitable combination of size and wavelength is critical to achieve single-mode operation and a better balance between mode confinement and propagation length.

## CONCLUSION

In conclusion, we have shown how a nearby dielectric substrate mediates the coupling of primary SPP modes on a metallic nanowire. The degree of interaction with the substrate can be controlled by changing the nanowire shape, gap, and refractive index of the substrate in order to achieve an improved balance between confinement and propagation length. For NWOS with a high-permittivity substrate, leaky radiation becomes dominant and raises the propagation losses significantly in the long-wavelength region. An optical barrier provided by a high-permittivity layer over a low-permittivity substrate can be used to block the leakage radiation. This simple layered substrate enables the NWOS to maintain high performance at the telecom wavelength. This finding paves the way for the fabrication of high-performance plasmonic waveguides by simply dropping a crystallized nanowire onto a flat dielectric substrate. Moreover, the NWOS configuration is compatible with the current semiconductor technology and is a prototype for deep subwavelength active devices. The reduced mode area can facilitate the interactions of SPPs with a quantum emitter, which makes the metallic nanowire an attractive quantum information transmission line.[50,51]

## METHODS

As a measure of the mode confinement for a plasmonic waveguide, the mode area $A$ should satisfy two criteria. First, it can be identifiable over the waveguide cross-section irrespective the geometry of the waveguide. Second, it contains a significant fraction of the total mode energy. In our calculations, $A$ is defined as a minima area that contains as much as $1 - 1/e^2$ of the total modal energy. The evaluation of $A$ is done numerically by integrating the area enclosed by a contour defined by a threshold energy density $W_0$. The value of $W_0$ is varied until the fraction of the modal energy within the contour reaches $1 - 1/e^2$, *i.e.*,

$$A = \int_{W \geq W_0} \mathrm{d}s$$

in which $W_0$ is determined by

$$\int_{W \geq W_0} W(\mathbf{r})\ \mathrm{d}s = \left(1 - \frac{1}{e^2}\right) \int_{S_\infty} W(\mathbf{r})\ \mathrm{d}s$$

$W(\mathbf{r}) = (1/4)\mathrm{Re}\{d[\varepsilon(\mathbf{r})\omega]/\mathrm{d}\omega\}|\mathbf{E}(\mathbf{r})|^2 + (1/4)\mu_0|\mathbf{H}(\mathbf{r})|^2$ is the energy density. $|\mathbf{E}(\mathbf{r})|^2$ and $|\mathbf{H}(\mathbf{r})|^2$ are the electric and magnetic field intensities, $\varepsilon(\mathbf{r})$ is the electric permittivity, and $\mu_0$ is the vacuum magnetic permeability.

The point dipole is modeled by an electric current segment, 1 nm in length, sitting 20 nm away from the center of the nanowire end-facet. The orientation of the segment represents the oscillation direction of the exciting dipole. The mesh grid was refined to 0.2 nm near the dipole to ensure accuracy. The simulation boundary is bounded by a PML layer to reduce reflection. The Joule heat plotted in Figure 2 and Figure 3 is integrated over the entire wire cross section with a 30 nm width in the $x$-direction.

*Conflict of Interest:* The authors declare no competing financial interest.

*Acknowledgment.* We thank Peter Nordlander for helpful discussions. This work was supported by MOST Grants (No. 2009CB930700), NSFC Grants (Nos. 10625418, 10874233, and 11004237), and the "Knowledge Innovation Project" (KJCX2-EW-W04) of CAS.

*Supporting Information Available:* Optical constants of Ag, dispersion relationship using Drude model, and the mode area calculated using another definition. This material is available free of charge *via* the Internet at http://pubs.acs.org.

## REFERENCES AND NOTES

1. Gramotnev, D. K.; Bozhevolnyi, S. I. Plasmonics beyond the Diffraction Limit. *Nat. Photonics* **2010**, *4*, 83–91.
2. Takahara, J.; Yamagishi, S.; Taki, H.; Morimoto, A.; Kobayashi, T. Guiding of a One-Dimensional Optical Beam with Nanometer Diameter. *Opt. Lett.* **1997**, *22*, 475–477.
3. Dickson, R. M.; Lyon, L. A. Unidirectional Plasmon Propagation in Metallic Nanowires. *J. Phys. Chem. B* **2000**, *104*, 6095–6098.
4. Krenn, J. R.; Lamprecht, B.; Ditlbacher, H.; Schider, G.; Salerno, M.; Leitner, A.; Aussenegg, F. R. Non Diffraction-Limited Light Transport by Gold Nanowires. *Europhys. Lett.* **2002**, *60*, 663–669.
5. Manjavacas, A.; de Abajo, F. J. G. Robust Plasmon Waveguides in Strongly Interacting Nanowire Arrays. *Nano Lett.* **2009**, *9*, 1285–1289.
6. Maier, S. A.; Kik, P. G.; Atwater, H. A.; Meltzer, S.; Harel, E.; Koel, B. E.; Requicha, A. A. G. Local Detection of Electromagnetic Energy Transport below the Diffraction Limit in

Metal Nanoparticle Plasmon Waveguides. *Nat. Mater.* **2003**, *2*, 229–232.
7. Moreno, E.; Rodrigo, S. G.; Bozhevolnyi, S. I.; Martín-Moreno, L.; García-Vidal, F. J. Guiding and Focusing of Electromagnetic Fields with Wedge Plasmon Polaritons. *Phys. Rev. Lett.* **2008**, *100*, 023901.
8. Bozhevolnyi, S. I.; Volkov, V. S.; Devaux, E.; Laluet, J.-Y.; Ebbesen, T. W. Channel Plasmon Subwavelength Waveguide Components including Interferometers and Ring Resonators. *Nature* **2006**, *440*, 508–511.
9. Dionne, J. A.; Sweatlock, L. A.; Atwater, H. A.; Polman, A. Plasmon Slot Waveguides: Towards Chip-Scale Propagation with Subwavelength-Scale Localization. *Phys. Rev. B* **2006**, *73*, 035407.
10. Oulton, R. F.; Sorger, V. J.; Genov, D. A.; Pile, D. F. P.; Zhang, X. A Hybrid Plasmonic Waveguide for Subwavelength Confinement and Long-Range Propagation. *Nat. Photonics* **2008**, *2*, 496–500.
11. Gramotnev, D. K.; Nielsen, M. G.; Tan, S. J.; Kurth, M. L.; Bozhevolnyi, S. I. Gap Surface Plasmon Waveguides with Enhanced Integration and Functionality. *Nano Lett.* **2012**, *12*, 359–363.
12. Oulton, R. F.; Sorger, V. J.; Zentgraf, T.; Ma, R. M.; Gladden, C.; Dai, L.; Bartal, G.; Zhang, X. Plasmon Lasers at Deep Subwavelength Scale. *Nature* **2009**, *461*, 629–632.
13. Sun, Y. G.; Xia, Y. N. Large-Scale Synthesis of Uniform Silver Nanowires Through a Soft, Self-Seeding, Polyol Process. *Adv. Mater.* **2002**, *14*, 833–837.
14. Tian, M. L.; Wang, J. U.; Kurtz, J.; Mallouk, T. E.; Chan, M. H. W. Electrochemical Growth of Single-Crystal Metal Nanowires *via* a Two-Dimensional Nucleation and Growth Mechanism. *Nano Lett.* **2003**, *3*, 919–923.
15. Ditlbacher, H.; Hohenau, A.; Wagner, D.; Kreibig, U.; Rogers, M.; Hofer, F.; Aussenegg, F. R.; Krenn, J. R. Silver Nanowires as Surface Plasmon Resonators. *Phys. Rev. Lett.* **2005**, *95*, 257403.
16. Sanders, A. W.; Routenberg, D. A.; Wiley, B. J.; Xia, Y. N.; Dufresne, E. R.; Reed, M. A. Observation of Plasmon Propagation, Redirection, and Fan-Out in Silver Nanowires. *Nano Lett.* **2006**, *6*, 1822–1826.
17. Pyayt, A. L.; Wiley, B.; Xia, Y. N.; Chen, A.; Dalton, L. Integration of Photonic and Silver Nanowire Plasmonic Waveguides. *Nat. Nanotechnol.* **2008**, *3*, 660–665.
18. Yan, R. X.; Pausauskie, P.; Huang, J. X.; Yang, P. D. Direct Photonic-Plasmonic Coupling and Routing in Single Nanowires. *Proc. Natl. Acad. Sci. U. S. A.* **2009**, *106*, 21045–21050.
19. Weeber, J. C.; Dereux, A.; Girard, C.; Krenn, J. R.; Goudonnet, J. P. Plasmon Polaritons of Metallic Nanowires for Controlling Submicron Propagation of Light. *Phys. Rev. B* **1999**, *60*, 9061–9068.
20. Fang, Y. R.; Li, Z. P.; Huang, Y. Z.; Zhang, S. P.; Nordlander, P.; Halas, N. J.; Xu, H. X. Branched Silver Nanowires as Controllable Plasmon Routers. *Nano Lett.* **2010**, *10*, 1950–1954.
21. Knight, M. W.; Grady, N. K.; Bardhan, R.; Hao, F.; Nordlander, P.; Halas, N. J. Nanoparticle-Mediated Coupling of Light into a Nanowire. *Nano Lett.* **2007**, *7*, 2346–2350.
22. Ma, Y. G.; Li, X. Y.; Yu, H. K.; Tong, L. M.; Gu, Y.; Gong, Q. H. Direct Measurement of Propagation Losses in Silver Nanowires. *Opt. Lett.* **2010**, *35*, 1160–1162.
23. Wei, H.; Li, Z.; Tian, X.; Wang, Z.; Cong, F.; Liu, N.; Zhang, S.; Nordlander, P.; Halas, N. J.; Xu, H. Quantum Dot-Based Local Field Imaging Reveals Plasmon-Based Interferometric Logic in Silver Nanowire Networks. *Nano Lett.* **2011**, *11*, 471–475.
24. Shegai, T.; Miljković, V. D.; Bao, K.; Xu, H.; Nordlander, P.; Johansson, P.; Käll, M. Unidirectional Broadband Light Emission from Supported Plasmonic Nanowires. *Nano Lett.* **2011**, *11*, 706–711.
25. Song, M. X.; Bouhelier, A.; Bramant, P.; Sharma, J.; Dujardin, E.; Zhang, D. G.; Colas-des-Francs, G. Imaging Symmetry-Selected Corner Plasmon Modes in Penta-Twinned Crystalline Ag Nanowires. *ACS Nano* **2011**, *5*, 5874–5880.
26. Fang, Z.; Fan, L.; Lin, C.; Zhang, D.; Meixner, A. J.; Zhu, X. Plasmonic Coupling of Bow Tie Antennas with Ag Nanowire. *Nano Lett.* **2011**, *11*, 1676–1680.
27. Kusar, P.; Gruber, C.; Hohenau, A.; Krenn, J. R. Measurement and Reduction of Damping in Plasmonic Nanowires. *Nano Lett.* **2012**, *12*, 661–665.
28. Zou, C. L.; Sun, F. W.; Xiao, Y. F.; Dong, C. H.; Chen, X. D.; Cui, J. M.; Gong, Q.; Han, Z. F.; Guo, G. C. Plasmon Modes of Silver Nanowire on a Silica Substrate. *Appl. Phys. Lett.* **2010**, *97*, 183102.
29. Li, Z. P.; Bao, K.; Fang, Y. R.; Guan, Z. Q.; Halas, N. J.; Nordlander, P.; Xu, H. X. Effect of a Proximal Substrate on Plasmon Propagation in Silver Nanowires. *Phys. Rev. B* **2010**, *82*, 241402.
30. Wang, Z. L.; Cowley, J. M. Surface-Plasmon Excitation for Supported Metal Particles. *Ultramicroscopy* **1987**, *21*, 77–93.
31. Malinsky, M. D.; Kelly, K. L.; Schatz, G. C.; Van Duyne, R. P. Nanosphere Lithography: Effect of Substrate on the Localized Surface Plasmon Resonance Spectrum of Silver Nanoparticles. *J. Phys. Chem. B* **2001**, *105*, 2343–2350.
32. Knight, M. W.; Wu, Y. P.; Lassiter, J. B.; Nordlander, P.; Halas, N. J. Substrates Matter: Influence of an Adjacent Dielectric on an Individual Plasmonic Nanoparticle. *Nano Lett.* **2009**, *9*, 2188–2192.
33. Zhang, S. P.; Bao, K.; Halas, N. J.; Xu, H. X.; Nordlander, P. Substrate-Induced Fano Resonances of a Plasmonic Nanocube: A Route to Increased-Sensitivity Localized Surface Plasmon Resonance Sensors Revealed. *Nano Lett.* **2011**, *11*, 1657–1663.
34. Chen, H. J.; Ming, T.; Zhang, S. R.; Jin, Z.; Yang, B. C.; Wang, J. F. Effect of the Dielectric Properties of Substrates on the Scattering Patterns of Gold Nanorods. *ACS Nano* **2011**, *5*, 4865–4877.
35. Vernon, K. C.; Funston, A. M.; Novo, C.; Gómez, D. E.; Mulvaney, P.; Davis, T. J. Influence of Particle-Substrate Interaction on Localized Plasmon Resonances. *Nano Lett.* **2010**, *10*, 2080–2086.
36. Albella, P.; Garcia-Cueto, B.; González, F.; Moreno, F.; Wu, P. C.; Kim, T. H.; Brown, A.; Yang, Y.; Everitt, H. O.; Videen, G. Shape Matters: Plasmonic Nanoparticle Shape Enhances Interaction with Dielectric Substrate. *Nano Lett.* **2011**, *11*, 3531–3537.
37. Johnson, P. B.; Christy, R. W. Optical-Constants of Noble-Metals. *Phys. Rev. B* **1972**, *6*, 4370–4379.
38. Dionne, J. A.; Sweatlock, L. A.; Atwater, H. A.; Polman, A. Planar Metal Plasmon Waveguides: Frequency-Dependent Dispersion, Propagation, Localization, and Loss beyond the Free Electron Model. *Phys. Rev. B* **2005**, *72*, 075405.
39. Oulton, R. F.; Bartal, G.; Pile, D. F. P.; Zhang, X. Confinement and Propagation Characteristics of Subwavelength Plasmonic Modes. *New J. Phys.* **2008**, *10*, 105018.
40. Buckley, R.; Berini, P. Figures of Merit for 2D Surface Plasmon Waveguides and Application to Metal Stripes. *Opt. Express* **2007**, *15*, 12174–12182.
41. Novotny, L.; Hafner, C. Light-Propagation in a Cylindrical Wave-Guide with a Complex, Metallic, Dielectric Function. *Phys. Rev. E* **1994**, *50*, 4094–4106.
42. Zia, R.; Selker, M. D.; Brongersma, M. L. Leaky and Bound Modes of Surface Plasmon Waveguides. *Phys. Rev. B* **2005**, *71*, 165431.
43. Zhang, S. P.; Wei, H.; Bao, K.; Håkanson, U.; Halas, N. J.; Nordlander, P.; Xu, H. X. Chiral Surface Plasmon Polaritons on Metallic Nanowires. *Phys. Rev. Lett.* **2011**, *107*, 096801.
44. Prodan, E.; Radloff, C.; Halas, N. J.; Nordlander, P. A Hybridization Model for the Plasmon Response of Complex Nanostructures. *Science* **2003**, *302*, 419–422.
45. Al-Bader, S. J.; Jamid, H. A. Diffraction of Surface Plasmon Modes on Abruptly Terminated Metallic Nanowires. *Phys. Rev. B* **2007**, *76*, 235410.
46. Miljković, V. D.; Shegai, T.; Johansson, P.; Käll, M. Simulating Light Scattering from Supported Plasmonic Nanowires. *Opt. Express* **2012**, *20*, 10816–10826.

47. Berini, P. Plasmon-Polariton Waves Guided by Thin Lossy Metal Films of Finite Width: Bound Modes of Asymmetric Structures. *Phys. Rev. B* **2001**, *63*, 125417.
48. Berini, P. Plasmon-Polariton Waves Guided by Thin Lossy Metal Films of Finite Width: Bound Modes of Symmetric Structures. *Phys. Rev. B* **2000**, *61*, 10484–10503.
49. Jung, J.; Søndergaard, T.; Bozhevolnyi, S. I. Theoretical Analysis of Square Surface Plasmon-Polariton Waveguides for Long-Range Polarization-Independent Waveguiding. *Phys. Rev. B* **2007**, *76*, 035434.
50. Chang, D. E.; Sørensen, A. S.; Hemmer, P. R.; Lukin, M. D. Quantum Optics with Surface Plasmons. *Phys. Rev. Lett.* **2006**, *97*, 053002.
51. Akimov, A. V.; Mukherjee, A.; Yu, C. L.; Chang, D. E.; Zibrov, A. S.; Hemmer, P. R.; Park, H.; Lukin, M. D. Generation of Single Optical Plasmons in Metallic Nanowires Coupled to Quantum Dots. *Nature* **2007**, *450*, 402–406.